# Predicting Magnetic Coupling and Spin-Polarization Energy in Triangulene Analogues

Hongde Yu,[1] Jianwei Sun,[2] Thomas Heine[1, 3, 4]*

[1]Faculty of Chemistry and Food Chemistry, TU Dresden, 01069 Dresden, Germany;

[2]Department of Physics and Engineering Physics, Tulane University, New Orleans, Louisiana 70118, United States;

[3]Institute of Resource Ecology, Helmholtz-Zentrum Dresden-Rossendorf, 04316 Leipzig, Germany;

[4]Department of Chemistry, Yonsei University and IBS CNM, Seoul 120-749, Korea.

*Corresponding author. Email: thomas.heine@tu-dresden.de.

## Abstract

Triangulene and its analogue metal-free magnetic systems have garnered increasing attention since their discovery. Predicting the magnetic couplings and spin polarization energy with quantitative accuracy is beyond the predictive power of today's density-functional theory (DFT) due to their intrinsic multi-reference character. Herein, we create a benchmark dataset of 25 magnetic systems with non-local spin densities, including the triangulene monomer, dimer, and their analogues. We calculate the magnetic coupling ($J$) and spin-polarization energy ($\Delta E_{spin}$) of these systems using complete active space self-consistent field (CASSCF) and coupled cluster methods as high-quality reference values. This reference data is then used to benchmark 22 DFT functionals commonly used in material science. Our results show that, while some functionals consistently correctly predict the qualitative character of the ground state, achieving quantitative accuracy with small relative errors is currently not feasible. PBE0, M06-2X, and MN15 are predicting the correct electronic ground state for all systems investigated here, and also have the lowest mean absolute error for predicting both $\Delta E_{spin}$ (0.34 eV, 0.32 eV and 0.31 eV) and $J$ (11.74 meV, 12.66 meV and 10.64 meV). They may therefore also serve as starting points for higher-level methods such as the *GW* or the random phase approximation. As other functionals fail for the prediction of the ground state, they cannot be recommended for metal-free magnetic

systems.

## Introduction:

Metal-free magnetism, as present in systems including molecular magnets,[1-2] covalent organic frameworks[3] and other organic polymers,[4] has attracted significant research interest in recent years. However, accurately predicting the magnetic interactions in these systems is challenging due to their intrinsic multi-reference nature, meaning that multiple spin-state configurations have small energy splittings.[5] To investigate magnetic interactions, researchers often turn to methods like density matrix renormalization group (DMRG), complete active space self-consistent field (CASSCF) and complete active space configuration interaction (CASCI), which can be enhanced with dynamic electron correlation methods like difference-dedicated configuration interaction (DDCI), complete active space second-order perturbation theory (CASPT2), and n-electron valence second-order perturbation theory (NEVPT2).[6-12] However, these approaches are computationally demanding and prohibitively expensive for large systems, including periodic structures. Density-functional theory (DFT) offers an alternative way to study the electronic structures of large systems, including periodic ones. Moreover, it provides a starting point for more advanced methods like *GW*[13-14] and the random phase approximation (RPA).[15-16] The quasi-particle description of DFT captures, in principle, static and dynamic correlations. To date, none of the existing functionals provides the quantitative accuracy and reliability to accurately assess the electronic configuration and energy differences in metal-free magnetic systems. A popular solution to improve the description of magnetic behavior in strongly correlated systems with metal centers, where the correlation is dominated by d electrons, is the DFT+*U* approach, which includes the empirical parameter Hubbard *U*. However, for metal-free systems, where static electron correlation cannot be associated with a well-defined subset of electrons, the DFT+*U* approach does not provide a viable solution.[6, 17] Therefore, it is beneficial to have a high-quality dataset with reliable benchmark data to assess the performance of a method for organic systems with non-local spin densities, which will also contribute to the research of two-dimensional polymers or covalent-organic frameworks within a periodic ansatz.

Triangulene (TRI) is the smallest polybenzenoid known with a triplet-ground state.[18-19] Recently, the realization of triangulene and its derivatives has led to the observation of many exotic phenomena including the Dirac cone and Haldane phase.[20-24] Compared to metal-organic complexes and diradicaloids with localized electronic structures, the delocalized and symmetric spin densities with extended π-conjugation make it a distinctive platform to explore electron correlation in metal-free magnets.[24] The magnetic coupling of triangulene has been studied using DFT (B3LYP functional) and CAS(4, 4), giving 160 meV and approximately 500 meV, respectively.[18-19, 25] B3LYP is the by far most often applied density-functional for describing organic molecules and widely used as standard method.[26] However, while it gives the correct sign of the magnetic coupling, it is a factor 3 off in its quantitative description.[18-19] Additionally, as dynamic electron correlation has rarely been considered in the reported multi-reference calculations of triangulenes, the available predictions for magnetic coupling may not be accurate.[19, 25] Therefore, it is of fundamental importance to thoroughly investigate the metal-free magnetism of triangulenes using advanced *ab initio* methods that take both static and dynamic electron correlations into account, and to evaluate the performance of available DFT functionals in predicting key parameters such as magnetic coupling and spin-polarization energy to open the door for periodic calculations, for example in two-dimensional (2D) polymers and covalent-organic frameworks (COFs).

In this work, we investigate the metal-free magnetism of triangulene and its analogues (see Figure 1) with advanced *ab initio* methods, i.e., with coupled cluster single-double and perturbative triple (CCSD(T)) and CASSCF/NEVPT2, which take into account both static and dynamic electron correlations. We first discuss in detail triangulene and its dimer, gaining fundamental insight into the magnetic interaction and electron correlation. Additionally, we create a comprehensive dataset of 25 metal-free magnetic systems with non-local spin densities They span a wide range of regimes in magnetic coupling and spin-polarization energy. These systems will serve as reliable references to evaluate the performance of various DFT functionals. Using these reference calculations, we benchmark 22 DFT functionals, covering generalized

gradient approximations (GGAs), meta-GGAs, hybrid GGAs, hybrid-meta GGAs, and range-separated hybrids. Our results show that, while achieving quantitative accuracy is still impossible, the hybrid functionals PBE0, MN15, and M06-2X produce qualitatively correct results with moderate deviations in energy, and are thus suitable starting points for methods such as the *GW* or the RPA.

**Results and Discussion:**

**1. Magnetic coupling and spin-polarization energy of triangulene monomer and dimer.**

Triangulene monomer is a prototypical non-Kekulé diradical with a triplet ground state. Its dimer is also a free radical with four unpaired electrons (Figure 2). In the dimer, triplet configuration of the monomers is maintained, and coupled in an anti-parallel alignment, resulting in an open-shell singlet (OSS) with $S = 0$.[19] In these diradicaloid and other radicals with an even number of unpaired electrons, the closed-shell singlet (CSS), the OSS and the high-spin state (HS), such as triplet or quintet, are the three important states to be considered (Figure 2). Among these states, the HS is well-represented by a single-determinant wavefunction, whereas the OSS is not, which poses a major challenge for computational chemistry. The relative energies of these three states are described by the spin-polarization energy $\Delta E_{spin}$ and the magnetic coupling $J$ (Figure 2). The spin-polarization energy is defined as the energy difference between high-spin open-shell and closed-shell states, $\Delta E_{spin} = E_{HS} - E_{CSS}$. This value will directly indicate whether the open-shell state is more stable, in other words, if the molecule is a radical. The magnetic coupling $J$ is derived from Heisenberg–Dirac–van Vleck (HDVV) Hamiltonian, $\widehat{H} = -J\widehat{S_1}\widehat{S_2}$, where $\widehat{S_1}$ and $\widehat{S_2}$ are the spin angular momentum operators on sites 1 and 2, respectively.[27] It is defined as the normalized energy difference between the low-spin OSS and high-spin states for triangulene monomer and dimer: $nJ = E_{OSS} - E_{HS}$, where n is 1 for the triplet (T) and 3 for the quintet (Q). For the triangulene monomer, the high-spin state is T and $J = E_{OSS} - E_T$, whereas it is Q for the dimer and $J = (E_{OSS} - E_Q)/3$.

The parameters $\Delta E_{spin}$ and $J$ are important metrics for understanding the magnetic

behavior of metal-free magnetism. $\Delta E_{spin}$ gives the magnitude of the electron correlation. A large $\Delta E_{spin}$ value signifies robust electron correlation and a stable spin-polarized state. In systems with partially-filled (quasi-)degenerate orbitals, the high-spin configuration is more stable than the closed-shell one due to the Coulomb repulsion of unpaired electrons according to Hund's rule.[27] $\Delta E_{spin}$ is related to the on-site Coulomb repulsion, $U$, of the Hubbard model, which is critical in the physics of strongly correlated systems.[28] It is also closely associated with Stoner magnetism, wherein the balance between electron correlation and electronic coupling underlies the origin of stable open-shell states and ferromagnetic interactions. We employ the domain-based local pair natural orbital coupled-cluster theory (DLPNO-CCSD(T)) method (see computational details section for more information) to calculate the energy difference between the closed-shell and high-spin states, i.e., triplet for the monomer and quintet for the dimer.[29] In comparison to the conventional CCSD(T) method, the DLPNO-CCSD(T) approach offers higher computational efficiency, capable to achieve nearly linear scaling while maintaining comparable accuracy. However, it cannot properly describe the OSS state due to its reliance on a restricted open-shell Hartree-Fock (ROHF) determinant rather than an unrestricted Hartree-Fock (UHF) one. Although conventional CCSD(T) is considered as a single-reference method, it is recognized as the golden standard in quantum chemistry and can robustly incorporate most dynamic electron correlations into the wave function. As shown in Table 1, the $\Delta E_{spin}$ is -1.39 eV for the monomer and -2.68 eV for the dimer, indicating that the open-shell high-spin states are generally more stable than the closed-shell ones. This manifests that these molecules are indeed open-shell radicals with strong electron correlation. It is worth noting that the $\Delta E_{spin}$ of the monomer is about half that of the dimer, as there are fewer free electrons and spin orbitals in the monomer. This reveals the close relationship between on-site Coulomb repulsion and spin-polarization energy.

As for $J$, it is of significance to evaluate the type and strength of magnetic interaction. If $J > 0$, the high-spin state is energetically favored, implying so-called ferromagnetic interaction (FM), whereas, if $J < 0$, the low-spin state is more stable for anti-ferromagnetic interaction (AFM). The ground state for the triangulene monomer is

a triplet, and thus $J > 0$, while for the dimer, it is the OSS and $J < 0$. It is notable that the low-spin state, i.e. the OSS radical with an even number of unpaired spins, has at least two Slater determinants with large coefficients. This makes single-determinant approaches such as HF, CCSD(T), and also DFT unsuitable for the accurate description of these systems. CASSCF is a natural approach to treat the multi-configurational systems with strong static correlation, where a full-CI expansion of the active space is generated, and the multi-configurational character is correctly considered. In order to obtain the $J$ value for the triangulene monomer and dimer, we performed the state-averaged CASSCF(12, 12) calculations as implemented in the ORCA program[30] (see computational details section for more information).

For the triangulene monomer, the triplet ground state is dominated by a single configuration 222221100000 of 79%, corresponding to $(\pi_1)^2(\pi_2)^2(\pi_3)^2(\pi_4)^2(\pi_5)^2(\pi^*_{s1})^1(\pi^*_{s2})^1(\pi^*_5)^0(\pi^*_4)^0(\pi^*_3)^0(\pi^*_2)^0(\pi^*_1)^0$, where $\pi^*_{s1}$ and $\pi^*_{s2}$ are two singly-occupied spin orbitals with anti-bonding characters. The natural orbitals in active space are shown in Figure S1. On the other hand, the significant contributions to the singlet state are the 222222000000 and 222220200000 configurations, which make up 41% and 39% of the states, respectively, while the open-shell singlet configurations contribute about 7%. These results demonstrate the multi-configurational character and strong static electron correlation in these systems, which arise from the degenerate spin orbitals. In addition, the two equally weighted closed-shell singlet configurations are more prominent in the monomer than the OSS configuration, possibly due to the weak coupling between the spin orbitals and the resulting super-exchange interaction, which is insufficient to stabilize the anti-ferromagnetic configuration. Afterwards, NEVPT2 calculations are performed on top of the CASSCF wave functions in order to include the dynamic electron correlations and obtain accurate values for $J$. The resulting energy difference between the singlet and triplet states of the monomer, $J$, was calculated to be 460 meV, indicating a very stable triplet ground state (Table 1).

As for the triangulene dimer, the high-spin state, quintet, is governed by the 222211110000 configuration of 85%. This configuration corresponds to $(\pi_1)^2(\pi_{1'})^2(\pi_2)^2(\pi_{2'})^2(\pi^*_{s1})^1(\pi^*_{s2})^1(\pi^*_{s3})^1(\pi^*_{s4})^1(\pi^*_{2'})^0(\pi^*_2)^0(\pi^*_{1'})^0(\pi^*_1)^0$. Among these

natural orbitals, ($\pi^*_{s1}$), ($\pi^*_{s2}$), ($\pi^*_{s3}$) and ($\pi^*_{s4}$) are four near-degenerated spin orbitals, while ($\pi_1$) and ($\pi_{1'}$) are pair of orbitals where only the sign of the wave function on one monomer is opposite. (Figure S2) By contrast, five configurations, 222211110000, 222222000000, 222220200000, 222202020000 and 222200220000, substantially contribute to the singlet state by 21%, 16%, 16%, 16% and 16% respectively. These results reveal the multiconfigurational nature of the singlet state, which originates from the four nearly degenerate spin orbitals. The NEVPT2 calculation gives an energy splitting between the singlet and the quintet of -23.64 meV and the *J* of -7.88 meV, indicating a stable OSS ground state and AFM interaction. For comparison, we also calculated the *J* value of the planar configuration, yielding -14.3 meV. This result is in good agreement with the experimental singlet-triplet gap of 14 meV for the triangulene dimer on the Au(111) surface.[19] It is noteworthy that, without considering dynamic electron correlations, the CASSCF calculations only predict about half of the value of *J*, -4.15 meV, for the dimer. This highlights the essential role of including dynamic electron correlations in the description of AFM interactions.

## 2. Magnetic coupling and spin-polarization energy of triangulenes dataset.

To obtain a more general understanding on the magnetic interactions of triangulenes, we created a collection of triangulene analogues as depicted in Figure 1, which cover a wide range of triangulene-centered radicals. In addition to triangulene monomer (TRI), they involve trioxotriangulene (TOT), triarylmethyl (TAM), nitrogen-doped triangulene (TRI(N)), boron-doped triangulene (TRI(B)) and phenalenyl (PLY). All these building units are stable radicals that have been synthesized in experiments except TRI(B). They are either directly connected into dimers or bridged by -C≡C- (CC), -C≡C-C≡C- (CCCC) and phenyl (Ph) linkages. These molecules are non-Kekulé diradicaloids with two unpaired electrons, except for the TRI-series that have four spins.

Afterwards, we employ similar approaches as for the triangulene monomer and dimer to calculate the $\Delta E_{spin}$ and the *J* of the whole collection and generate a

triangulenes magnetism dataset (see computational details). We found that all the molecules, except for triangulene monomer, have OSS ground states and AFM interactions with $J < 0$ (Table 2). Our results show that the triangulene-based molecules exhibit a wide range of magnetic properties, with the $\Delta E_{spin}$ and $J$ values ranging from -2.73 eV to -0.34 eV and from -203 meV to -1.0 meV, respectively (Figure 3 and Table 2). These molecules can be broadly classified into three categories based on their $\Delta E_{spin}$ and $J$ values: those with strong $J$ and weak $\Delta E_{spin}$ (mostly TOT and TAM series), those with weak $J$ and weak $\Delta E_{spin}$ (TRI(N), TRI(B), and PLY series), and those with weak $J$ and strong $\Delta E_{spin}$ (TRI series). For all the diradicals, the orbitals in their active space follow the pattern of $(\pi_1)(\pi_{1'})(\pi_2)(\pi_{2'})(\pi^*_{s1})(\pi^*_{s2})(\pi^*_{2'})(\pi^*_2)(\pi^*_{1'})(\pi^*_1)$ due to orbital degeneracy imposed by symmetry resulting from the equivalence of the monomers (Figures S3-25). For the TRI-Ph molecule, the experimental singlet-triplet energy gap of 2 meV data is available[19] and closely matches our calculation of the $J$ value (Table 2). For the systems sharing the same building units, similar $\Delta E_{spin}$ are observed, manifesting the spin-polarization is principally defined by the elementary monomer (Table 2). We also observe that the molecules bridged by -C≡C- have stronger magnetic coupling than those bridged by -C≡C-C≡C-, indicating the locality of magnetic interactions despite being mediated by the conjugated linkages. However, the directly-linked dimers do not necessarily have stronger $J$ than the -C≡C- linked ones due to loss of conjugation across their twisted dimer linkages. The spin ladder of all the dimer molecules is shown in Figure S26.

From a materials design perspective, the AFM interaction originates from the super-exchange between the monomers and can be described by $-4t^2/U$, where $t$ represents the hopping integral in the Hubbard model. Thus, increasing the conjugation across the molecule can enhance the electronic coupling and lead to stronger AFM interactions. Factors such as planarity and linkages can greatly affect the conjugation, as we have seen that the $J$ value of the TRI dimer increases from -7.88 meV to -14.3 meV when transformed from a distorted to a planar configuration. With regards to electron correlation, an increase in the number of unpaired electrons and degenerate frontier orbitals will generate a greater Coulomb repulsion between the spins located on the same monomer, as the TRI dimer with four unpaired electrons has a larger $\Delta E_{spin}$

than other diradicaloids with two unpaired electrons (Table 2). As a result, the search for non-Kekule building blocks, such as Clar's goblet[31] and other triangulene systems[32] with unpaired π-electrons, holds great promise for the discovery of metal-free magnetism with strong electron correlation.

## 3. Benchmark of broken-symmetry DFT functionals for triangulene dataset.

Instead of a multiconfigurational wave function in CASSCF or CASCI, the broken-symmetry (BS) DFT is also a popular and well-established approach to tackle the open-shell states, and the approach is feasible even for relatively large systems.[33-35] However, the accuracy of BS-DFT depends on the exchange-correlation functional being used.[36] In order to evaluate the reliability of different functionals, we will compare the results obtained from BS-DFT with our references for $J$ and $\Delta E_{spin}$ (see computational details). Here, $\Delta E_{spin}$ is defined as $\Delta E_{spin} = E_{HS} - E_{CSS}$, where $E_{HS}$ and $E_{CSS}$ are calculated by unrestricted and restricted DFT, respectively. However, the OSS is the ground state for nearly all the molecules in the dataset, rather than the high-spin or closed-shell state. This makes it essential to accurately calculate $J$ in order to understand the magnetic properties of these molecules. However, how to properly extract $J$ from BS-DFT calculations pertaining to OSS remains a contentious issue.[37-39] Numerous mapping schemes have been proposed, wherein three are commonly discussed and employed, i.e. Noodleman's (eqn. (1)),[34] Yamaguchi's (eqn. (2)),[40-41] and Ruiz's (eqn. (3)) approaches,[36] as follows:

$$J = \frac{-2(E_{\mathrm{HS}} - E_{\mathrm{OSS}})}{S_{max}^2} \quad (1)$$

$$J = \frac{-2(E_{\mathrm{HS}} - E_{\mathrm{OSS}})}{\langle S^2 \rangle_{\mathrm{HS}} - \langle S^2 \rangle_{\mathrm{LS}}} \quad (2)$$

$$J = \frac{-2(E_{\mathrm{HS}} - E_{\mathrm{OSS}})}{S_{max}(S_{max}+1)} \quad (3)$$

Where $S_{max}$ is the total spin of the HS state, $\langle S^2 \rangle_{\mathrm{HS}}$ and $\langle S^2 \rangle_{\mathrm{LS}}$ are the expectation values for the total spin of the HS and LS states, respectively. Among them, both Noodleman's and Yamaguchi's methods are spin-projected approaches, while Ruiz's method is referred to as a non-projected approach.[37] Although some discussions have focused on selecting mapping approaches based on the strength of $J$, it is important to

note that the fundamental understanding of OSS calculated by BS-DFT varies inherently across these approaches.[39, 42] The long-standing debate regarding which mapping approach can yield more reliable results has yet to reach a consensus within the community.[37-38, 43] In practice, the choice of approach is contingent on the specific chemical system under investigation and the functional employed.[38] Each method has been supported by experimental data or high-level quantum chemistry calculations in the literature.[36-38] This further complicates the prediction of *J* with quantitative accuracy using BS-DFT. In this study, rather than endorsing a particular approach, we calculated *J* using all three formulas, with the results presented in Table S1 (Noodleman's approach), Table S2 (Yamaguchi's approach), and Tables 1-2 (Ruiz's approach).

We firstly benchmark 22 DFT functionals for the triangulene monomer and dimer, including PBE,[44] BLYP,[45-46] BP86,[45, 47] TPSS,[48] M06L,[49] SCAN,[50] r$^2$SCAN-3c,[51] MN15-L,[52] B3LYP,[46, 53] PBE0,[46, 54] M06-2X,[52] TPSSh,[48] MN15,[55] PW6B95,[56] ωB97XD,[57] ωB97M-V,[58] HSE06,[59] B2GP-PLYP,[60] PWPB95,[61] B2PLYP,[62] and ωB97X-2[63] (Table 1). This comprehensive selection of functionals covers GGA, meta-GGA, hybrid-GGA, hybrid-meta GGA, range-separated hybrids, and double hybrids. The total energy of CSS, OSS and HS, namely triplet for the monomer and quintet for the dimer, are calculated, and *J* and $\Delta E_{spin}$ are derived. For OSS states, the broken-symmetry approach is employed, while the stability of DFT wavefunction is tested. As in Gaussian 16 it is possible to automatically optimize the wavefunction until it is stable, most of the calculations are performed employing this code, except for SCAN, r$^2$SCAN-3c, ωB97M-V, ωB97X-2, B2GP-PLYP, and PWPB95, which are not available in Gaussian 16. Instead, these functionals have been studied using the ORCA 5.0 program. We used this occasion to compare the numerical differences between the Gaussian 16 and ORCA 5.0 programs. Even though the numerical values of *J* and $\Delta E_{spin}$ correspond to small energies, the calculations at B3LYP/def2-TZVP level are consistent for all cases studied with difference of the target quantities within 2% (Table S3). As shown in Figure 4 and Table 1, the hybrid functionals generally provide a more accurate prediction of the *J* and $\Delta E_{spin}$ with MAE of 110.1 meV and 0.25 eV for the monomer and 1.7 meV and 0.74 eV for the dimer compared to those from GGA and meta-GGA

functionals of 218.6 meV and 0.50 eV for the monomer and 3.9 meV and 1.7 eV for the dimer. Among them, for the dimer, PBE0, MN15 and ωB97M-V give the best prediction of -9.73 meV, -8.90 meV and -10.07 meV for the $J$ and -1.99 eV, -2.40 eV and -2.80 eV for the $\Delta E_{spin}$ with reference to -7.88 meV for the $J$ and -2.68 eV for the $\Delta E_{spin}$. As for the monomer, ωB97XD and ωB97M-V predict the $J$ values of 449.52 meV and 455.30 meV and $\Delta E_{spin}$ of -1.46 eV, which are comparable to the reference values of 460 meV and -1.39 eV. On the contrary, apart from SCAN series of functionals, most GGA and meta-GGA functionals severely underestimate both the $J$ and the $\Delta E_{spin}$ with a mean relative error of -59% and -45% for the monomer and -50% and -71% for the dimer. Particularly, SCAN works surprisingly well for the triangulene monomer and predicts the $J$ of 468.41 meV and $\Delta E_{spin}$ of -1.4 eV, yet less accurately for the dimer with relative errors of 119% and -24%. This suggests that SCAN may be suitable to describe systems with strong magnetic coupling. It is also observed that double hybrid functionals generally produce unreliable results for both the monomer and dimer, potentially leading to incorrect ground states[64] (Table 1 and Figure 4). For example, B2GP-PLYP and ωB97X-2 erroneously predict an OSS ground state for the monomer and a high-spin state for the dimer. Although B2PLYP could correctly indicate the ground state, the $J$ values are overestimated by 23% and 216% for the monomer and dimer, respectively.

On the basis of these findings, we further choose 10 functionals with better popularity in material science, including PBE, SCAN, r$^2$SCAN-3c, B3LYP, PBE0, M06-2X, MN15, ωB97XD, ωB97X-V and HSE06, and extend above-mentioned DFT calculations to all the molecules in the dataset. Based on our benchmark results shown in Table 2 and Figure 5, we found that while the qualitative predictions of $J$ and $\Delta E_{spin}$ are generally good, quantitative predictions are not yet attainable within the DFT framework, particularly for the systems with relatively weak magnetic coupling and spin-polarization, such as -2 meV for $J$ and -0.5 eV for $\Delta E_{spin}$, where errors in the relative energies between different states are largest. Regarding the mapping approaches, we found that Noodleman's and Yamaguchi's methods yield similar $J$ values, which are generally about twice those predicted by Ruiz's method. (Tables S1-

2 and Table 2) For example, the predicted *J* values for TRI dimer are -10.08 meV, -10.53 meV, and -6.76 meV using Noodleman's, Yamaguchi's, and Ruiz's methods, respectively, in comparison to the reference value of 7.88 meV. This overestimation of *J*, as predicted by Noodleman's and Yamaguchi's approaches, has been consistently reported in the literature, particularly for organic diradical systems.[65-67] Consequently, scaling factors of 0.3-0.5 have been employed to align with experimental *J* values.[68-70] As demonstrated in Figure S27, Tables S1-2 and Table 2, *J* predictions derived from Noodleman's and Yamaguchi's methods exhibit larger mean absolute errors (MAEs) and mean relative errors (MREs) than those obtained using Ruiz's approach. For example, with B3LYP, PBE0, and M062X functionals, the MAEs are 29.6 meV, 34.43 meV, and 21.75 meV for Noodleman's method, 25.92 meV, 34.62 meV, and 21.86 meV for Yamaguchi's method, and 13.38 meV, 11.74 meV, and 12.66 meV for Ruiz's approach. Thus, at least from a numerical perspective, Ruiz's method appears more suitable for extracting *J* from BS-DFT for these metal-free systems.[66-67, 71-72] Hereafter, the detailed analysis of the functionals' performance will be grounded in the results obtained using Ruiz's approach.

Among the tested functionals, the PBE0, M06-2X and MN15 are most accurate both for *J* and $\Delta E_{spin}$, with MAE of 11.74 meV, 12.66 meV and 10.64 meV for *J* and 0.34 eV, 0.32 eV and 0.31 eV for $\Delta E_{spin}$. The MRE are 15%, -30%, 0% for *J* and -4%, 29% and 21% for $\Delta E_{spin}$ (Table 2 and Figure 5). The root mean square error (RMSE) and mean absolute relative error (MARE) are also shown in Table 2. Although the MAE of B3LYP and HSE06, i.e. 13.38 meV and 13.18 meV for *J* and 0.46 eV and 0.41 eV for $\Delta E_{spin}$, are comparable to that of PBE0 and M06-2X, they incorrectly predict the relative energy of closed-shell and high-spin state for TAM dimer, resulting in erroneous $\Delta E_{spin}$ (Table 2). These results demonstrate that PBE0, M06-2X and MN15 generally provide a more accurate and reliable description of the magnetic systems compared to other functionals. In addition, SCAN, as meta-GGA functional, shows similar accuracy as many hybrid functionals, especially for the prediction of $\Delta E_{spin}$, where the MAE and MRE are 0.36 eV and -11%. This provides a significant computational advantage in optimizing the magnetic state for large systems, especially

for high-spin states, as meta-GGA functionals are generally less computationally expensive. However, some functionals mistake the sign of $J$ and $\Delta E_{spin}$, leading to an incorrect prediction of the ground state. For example, PBE will reverse the sign of the $J$ for all the TRI(B) series molecules and the sign of $\Delta E_{spin}$ for all the TAM and most of the TOT molecules (Table 2). Although ωB97XD and ωB97X-V correctly predict the signs of $J$ and $\Delta E_{spin}$ for all the molecules in the dataset, the MRE of $\Delta E_{spin}$ are 104% and 113%, which is about three times larger than other hybrid functionals, indicating severe overestimation of electron correlation. The $\langle S^2 \rangle_{\mathrm{HS}}$ and $\langle S^2 \rangle_{\mathrm{LS}}$ of all these functionals for the molecules in the dataset are shown in Table S4. The spin densities of all the dimer molecules calculated by MN15 functional are shown in Figures S27-S50 Optimizing the range-separation parameter ω, rather than using a single value for all the systems, may lead to a more accurate description of magnetic states, as this has been demonstrated to enhance the prediction of the fundamental gaps and the charge-transfer excitations in organic assemblies and polymers.[73] Furthermore, previous research has demonstrated that LC-ωPBE improves the description of magnetic coupling in transition-metal oxides compared to B3LYP.[74] In view of the direct impact on the electron correlations, we calculated $J$ and $\Delta E_{spin}$ with long-range (LC) corrected hybrid functional, LC-ωPBE,[75-77] and employ different values of ω based on the building monomers, where ω=0.20 for TRI, ω=0.15 for TOT, TAM and PLY, ω=0.10 for TRI(N) and ω=0.05 for TRI(B) were chosen. The results are shown in Table 2 and Figure 5 and denoted as LC-ωPBE* in comparison to LC-ωPBE with default ω (ω = 0.4). By using these target application-tuned values of ω, we significantly improve the values for $\Delta E_{spin}$ with MAE and MRE of 0.13 eV and -0.02% compared with that of 0.73 eV and 82% in LC-ωPBE with default ω as well as other hybrid functionals. Also, its values for $J$ with MAE and MRE of 13.13 meV and -25% are comparable to those calculated with PBE0 and M06-2X. This demonstrates the effectivity of range-separated hybrid functionals for strong-correlated systems, however, the range-separation parameter must be adjusted based on the electron correlations in order to achieve accurate predictions. This may be a suitable approach for studying oligomers or polymers based on the same monomer. Current developments for optimizing the

range-separation parameter based on Koopman's theorem might provide useful alternatives in the future and a generalized multireference-DFT method could also give more accurate predictions.[73, 78-81]

## Conclusion

In summary, we investigated the magnetic properties of triangulene monomer, dimer and their analogues, and predicted their spin-polarization energy ($\Delta E_{spin}$) and magnetic coupling ($J$) with DLPNO-CCSD(T) and CASSCF/NEVPT2 methods. Our predictions of $J$ for the triangulene dimer with and without the phenylene spacer, i.e. -7.88 meV and -2.42 meV, are consistent with experimental observations. We highlight the importance of including both dynamic and static correlations for the accurate calculation of magnetic interactions. We found that all the molecules, except the triangulene monomer, have open-shell-singlet ground states and AFM interactions with $J < 0$. On the basis of these results, we suggest a comprehensive dataset with high-quality reference values, containing 25 metal-free magnetic molecules. This dataset covers a wide range of $\Delta E_{spin}$ from -2.73 eV to -0.34 eV and $J$ from -203 meV to -1.0 meV, which provides an extensive and reliable starting point for future research. In order to assess the performance of DFT functionals for the prediction of $\Delta E_{spin}$ and $J$, we benchmarked 22 functionals for the triangulene monomer and dimer, and 10 functionals for the whole dataset. We found that, although qualitative prediction of $\Delta E_{spin}$ and $J$ could be achieved within the DFT framework by carefully choosing the functionals, quantitative accuracy has not been reached yet, especially for systems with relatively weak electron correlations. In general, PBE0, M06-2X and MN15 are recommended for calculating both $J$ and $\Delta E_{spin}$ of metal-free magnetic systems, as they have reasonable MAE of 11.74 meV, 12.66 meV and 10.64 meV respectively for $J$ and 0.34 eV, 0.32 eV and 0.31 eV respectively for $\Delta E_{spin}$. On the contrary, most GGA and meta-GGA functionals will underestimate both parameters, for example, PBE with MRE of -144% and -78% for $J$ and $\Delta E_{spin}$ respectively. SCAN performs as accurately as many hybrid functionals for $\Delta E_{spin}$ with MAE of 0.36 eV, and produces an accurate

value for $J$ of the triangulene monomer with a relative error of 2%, indicating its potential for describing systems with strong magnetic coupling and spin-polarization. We further demonstrated that tuning the range-separation parameter, ω, based on the electron correlation in the range-separated hybrid functional, LC-ωPBE, improves the performance, particularly for $\Delta E_{spin}$. Our findings will be used to advance the understanding of the magnetic interactions and spin-polarization of triangulene and its analogues and illustrate the performance of novel DFT functionals when describing metal-free magnetism.

## Computational details

The geometries of all the molecules have been optimized at the PBE0/def2-TZVP level as implemented in the Gaussian16 program.[82] We have performed the domain-based local pair natural orbital coupled-cluster theory (DLPNO-CCSD(T)) with ORCA 5.0 program.[30] "RIJCOSX" method has been employed to speed up the SCF process. The auxiliary basis set, def2-TZVP/C, and Coulomb fitting set, def2/J, have been used for correlated calculations.[83] TightSCF option has been used to tighten the convergence settings. The closed-shell singlet and quintet states have been calculated for TRI dimer, TRI-CC, TRI-CCCC and TRI-Ph, while the closed-shell singlet and triplet states have been calculated for the other molecules in the dataset.

The state-averaged (SA) CASSCF has also been carried out with ORCA 5.0 program to calculate the magnetic coupling. SA CASSCF is more convenient and computationally efficient to conduct a constrained minimization of a weighted sum of energies pertaining multiple electronic states, whereas the state-specific (SS) CASSCF approach often encounters convergence issues due to root flipping. Thus, SA CASSCF provides a more balanced treatment of multiple states and is better suited for studying magnetic interactions.[84] RIJK approximation has been used to speed up the SCF calculations. The exchange fitting basis, def2/JK, has been used.[85] The singlet and quintet states have been considered for TRI dimer, TRI-CC, TRI-CCCC, and TRI-Ph, while the singlet and triplet states have been calculated for the other molecules in the

dataset because the TRI-series dimers possess 4 unpaired electrons, while the other diradicals only have 2 spins. Considering the degeneracy of the orbitals, CAS(12, 12) has been used for TRI monomer, TRI dimer, TRI-CC, TRI-CCCC, TRI-Ph, while CAS(10, 10) has been used for the other diradicals. This means, for all the molecules in the dataset, we have applied a consistent active space, includes 4 occupied orbitals, 4 virtual orbitals, and all the SOMOs. While it would be ideal to include all the π-electrons in the active space, the resources required for this scale exponentially and make CAS(14,14) calculations impractical. In addition, adding nearly fully occupied or virtual orbitals to the active space may lead to convergence problems.[86] On top of the CASSCF-optimized wave function, the RI-NEVPT2 method has been employed to include the dynamic correlation. We have noticed major progress in the development of density matrix renormalization group (DMRG) technique recently, allowing for the inclusion of more orbitals and electrons in the active space.[8-9] This improvement leads to enhanced accuracy that aligns with experimental data, particularly for systems containing numerous SOMOs and necessitating large active spaces, such as the chromium dimer, where notable discrepancies between experimental and computational data have been reported. In this study, we stick to the more traditional ab initio methods as they are sufficient for the small number of SOMOs and show excellent agreement to experiment if available.

For DFT calculations, SCAN, r$^2$SCAN-3c, wB97M-V, ωB97X-2, B2GP-PLYP, and PWPB95 calculations have been performed in ORCA 5.0 program, while the other functionals have been carried out with Gaussian 16 program. For closed-shell singlet, restricted DFT calculations have been performed, while unrestricted DFT calculations have been employed for the triplet and quintet. For open-shell singlet, a broken-symmetry approach has been performed. The stability of the DFT wave function has been optimized and checked with “stable=opt” for Gaussian and “STABPerform true” for ORCA. The basis set is def2-TZVP for all the calculations considering the large computational demand for the CAS and CCSD(T) calculations.[87] Mean absolute relative error (MARE) is defined as $\mathrm{MARE} = \frac{1}{\mathrm{n}}\sum_{i\leq n}\left|\frac{x_i - x_{\mathrm{ref}}}{x_{\mathrm{ref}}}\right|$. Mean relative error

(MRE) is defined as $\mathrm{MRE} = \frac{1}{\mathrm{n}}\sum_{i\leq n}(\frac{x_i - x_{\mathrm{ref}}}{x_{\mathrm{ref}}})$. Mean absolute error (MAE) is defined as $\mathrm{MAE} = \frac{1}{\mathrm{n}}\sum_{i\leq n}|x_i - x_{\mathrm{ref}}|$. Root mean square error (RMSE) is defined as $\mathrm{RMSE} = \sqrt{\frac{1}{\mathrm{n}}\sum_{i\leq n}(x_i - x_{\mathrm{ref}})^2}$.

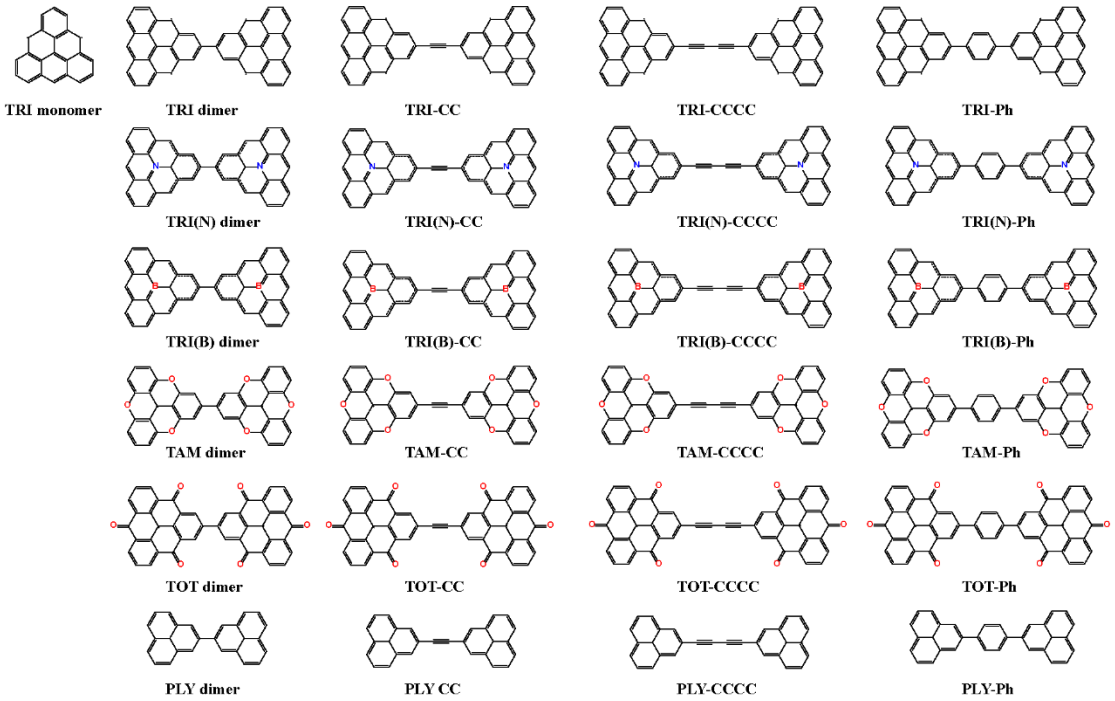


**Figure 1. Molecule collection of triangulene monomer, dimer and its analogues.**

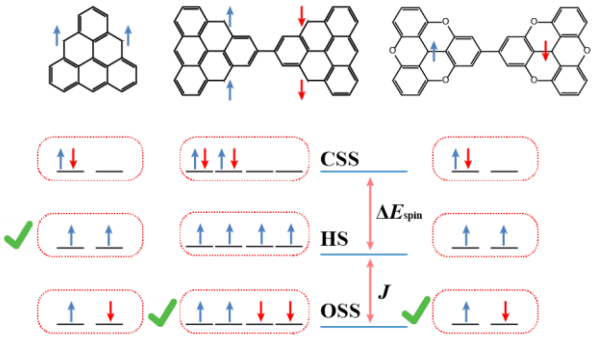


**Figure 2. Molecular structures and spin states of triangulene monomer, dimer and TAM dimer. CSS: closed-shell singlet, OSS: open-shell singlet, HS: high-spin state, namely triplet for triangulene monomer and TAM dimer and quintet for triangulene dimer. The green check signs indicate the ground states.**

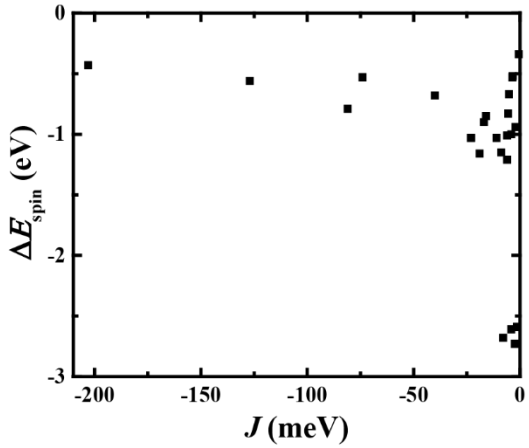


**Figure 3. Magnetic coupling and spin-polarization energy distribution of the dataset.**

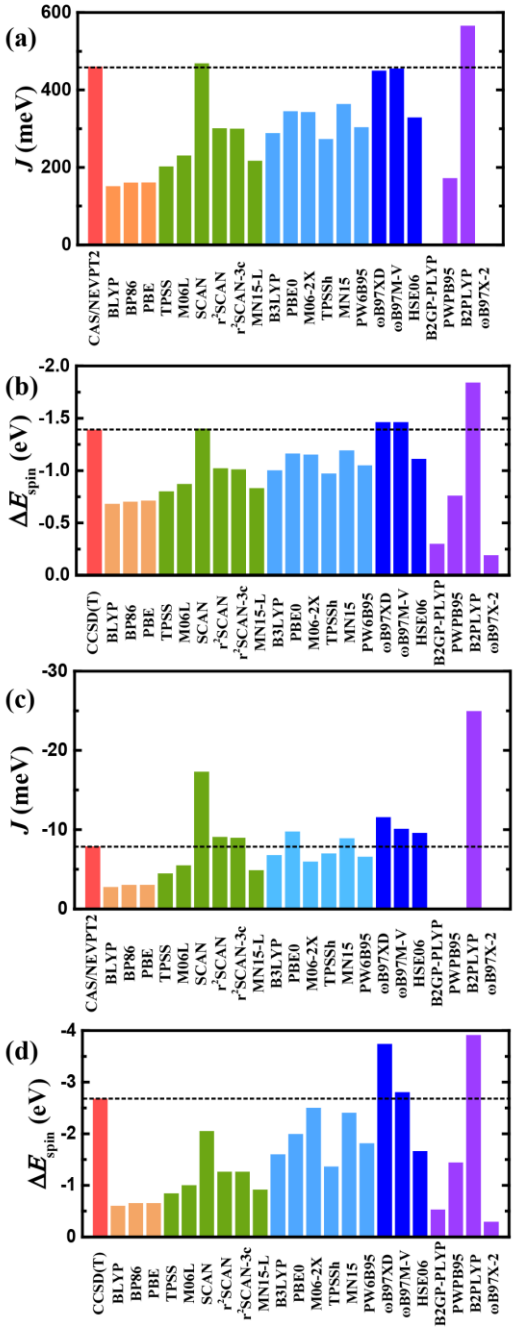


**Figure 4. Magnetic coupling, *J*, (a) and spin-polarization energy, $\Delta E_{spin}$, (b) of the triangulene monomer, as well as *J* (c) and $\Delta E_{spin}$ (d) of the dimer. The reference is highlighted in red. The negative values of *J* in (a) and positive values in (c) are not shown. Color code: reference value in red; GGAs in orange; meta-GGAs in green; hybrid functionals in light blue; range-separated hybrids in blue; double hybrids in purple.**

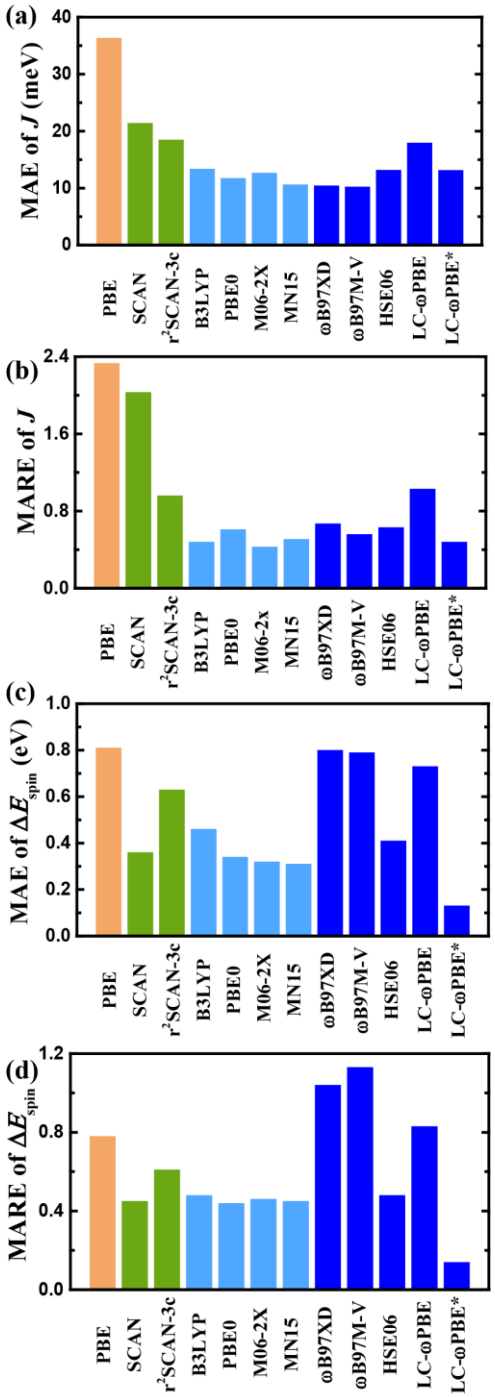


**Figure 5. Mean absolute error (MAE) (a) and mean absolute relative Error (MARE) (b) of *J*, as well as MAE (c) and MARE (d) of $\Delta E_{spin}$. The ω is tuned according to the electron correlations in LC-ωPBE*, and ω is 0.4 by default in LC-ωPBE. Color code: GGA in orange; meta-GGAs in green; hybrid functionals in light blue; range-separated hybrids in blue.**

**Table 1. Benchmark of DFT functionals of the magnetic coupling and spin-polarization energy for triangulene monomer and dimer.**

| | | Monomer | | Dimer | |
|---|---|---|---|---|---|
| | | $J$ (meV) | $\Delta E_{spin}$ (eV) | $J$ (meV) | $\Delta E_{spin}$ (eV) |
| Reference | | 460 | -1.39 | -7.88 | -2.68 |
| GGA | BLYP | 150.91 | -0.68 | -2.74 | -0.60 |
| | BP86 | 160.21 | -0.70 | -2.99 | -0.65 |
| | PBE | 160.57 | -0.71 | -3.00 | -0.65 |
| Meta-GGA | TPSS | 202.13 | -0.80 | -4.47 | -0.84 |
| | M06L | 230.05 | -0.87 | -5.49 | -1.00 |
| | SCAN | 468.41 | -1.40 | -17.29 | -2.05 |
| | r$^2$SCAN | 300.71 | -1.02 | -9.05 | -1.26 |
| | r$^2$SCAN-3c | 299.87 | -1.01 | -8.95 | -1.26 |
| | MN15-L | 216.65 | -0.83 | -4.87 | -0.91 |
| Hybrid | B3LYP | 288.39 | -1.01 | -6.76 | -1.60 |
| GGA | PBE0 | 344.73 | -1.16 | -9.73 | -1.99 |
| Hybrid | M06-2X | 342.57 | -1.15 | -5.94 | -2.50 |
| meta-GGA | TPSSh | 273.15 | -0.97 | -6.97 | -1.36 |
| | MN15 | 363.28 | -1.19 | -8.90 | -2.40 |
| | PW6B95 | 303.27 | -1.05 | -6.56 | -1.81 |
| Range- | ωB97XD | 449.52 | -1.46 | -11.56 | -3.74 |
| separated | ωB97M-V | 455.30 | -1.46 | -10.07 | -2.80 |
| Hybrids | HSE06 | 328.50 | -1.11 | -9.56 | -1.66 |
| Double | B2GP-PLYP | -88.91 | -0.30 | 16.47 | -0.53 |
| Hybrids | PWPB95 | 171.69 | -0.76 | 2.21 | -1.44 |
| | B2PLYP | 565.61 | -1.84 | -24.94 | -3.91 |
| | ωB97X-2 | -161.67 | -0.19 | 18.74 | -0.29 |

**Table 2. Benchmark of DFT functionals of the magnetic coupling and spin-polarization energy for the molecules in the dataset.**

| $J$(meV) / $\Delta E_{spin}$(eV) | | Ref. | PBE | SCAN | r$^2$SCAN-3c | B3LYP | PBE0 | M062X | MN15 | ωB97XD | ωB97M-V | HSE06 | LC-ωPBE | LC-ωPBE* |
|---|---|---|---|---|---|---|---|---|---|---|---|---|---|---|
| **TRI mono** | ***J*** | **460** | 160.57 | 468.41 | 299.87 | 288.39 | 344.73 | 342.57 | 363.28 | 449.52 | 455.3 | 328.5 | 610.88 | 378.81 |
| | $\Delta E_{spin}$ | **-1.39** | -0.71 | -1.4 | -1.01 | -1.01 | -1.16 | -1.15 | -1.19 | -1.46 | -1.46 | -1.11 | -2.04 | -1.27 |
| **TRI dimer** | ***J*** | **-7.88** | -3 | -17.29 | -8.95 | -6.76 | -9.73 | -5.94 | -8.9 | -11.56 | -10.07 | -9.56 | -23.14 | -7.72 |
| | $\Delta E_{spin}$ | **-2.68** | -0.65 | -2.05 | -1.26 | -1.6 | -1.99 | -2.5 | -2.4 | -3.74 | -2.8 | -1.66 | -5.21 | -3.24 |
| **TRI-CC** | ***J*** | **-4.13** | -2.08 | -16.39 | -7.6 | -5.27 | -7.91 | -4.33 | -6.79 | -9.27 | -7.66 | -7.75 | -19.72 | -6.21 |
| | $\Delta E_{spin}$ | **-2.61** | -1.26 | -2.11 | -1.31 | -1.74 | -2.16 | -2.34 | -2.42 | -4.27 | -2.85 | -2.12 | -4.16 | -2.58 |
| **TRI-CCCC** | ***J*** | **-1.33** | -1.24 | -12.02 | -4.84 | -3.16 | -4.94 | -2.33 | -4.08 | -5.63 | -4.3 | -4.85 | -13.24 | -3.72 |
| | $\Delta E_{spin}$ | **-2.59** | -1.22 | -2.13 | -1.32 | -1.92 | -2.18 | -2.36 | -2.25 | -3 | -2.82 | -2.27 | -4.2 | -2.6 |
| **TRI-Ph** | ***J*** | **-2.42** | -0.36 | -6.63 | -1.12 | -0.94 | -1.45 | -0.73 | -1.24 | -1.6 | -1.28 | -1.45 | -1 | -1 |
| | $\Delta E_{spin}$ | **-2.73** | -1.38 | -2.12 | -1.32 | -1.78 | -2.2 | -2.26 | -2.43 | -2.97 | -2.99 | -2.12 | -2.58 | -2.58 |
| **TRI(N) dimer** | ***J*** | **-2.1** | 26.07 | 0.08 | -1.53 | -0.38 | -0.33 | -0.21 | -0.18 | -0.19 | -0.19 | -0.36 | -0.2 | -0.3 |
| | $\Delta E_{spin}$ | **-0.94** | -0.31 | -0.84 | -0.52 | -0.73 | -0.92 | -1.14 | -1.11 | -1.69 | -1.8 | -0.78 | -1.41 | -0.74 |
| **TRI(N)-CC** | ***J*** | **-16** | -5.2 | -40.66 | -22.82 | -15.81 | -22.15 | -13.74 | -18.76 | -23.51 | -19.49 | -21.92 | -17.12 | -9.48 |
| | $\Delta E_{spin}$ | **-0.85** | -0.29 | -0.83 | -0.52 | -0.73 | -0.93 | -1.22 | -1.16 | -1.9 | -2.04 | -0.78 | -1.61 | -0.82 |
| **TRI(N)-CCCC** | ***J*** | **-6.04** | -4.28 | -31.92 | -47.15 | -10.11 | -14.57 | -7.77 | -11.78 | -14.85 | -11.39 | -14.56 | -10.73 | -5.94 |
| | $\Delta E_{spin}$ | **-1.01** | -0.29 | -0.85 | -0.5 | -0.78 | -0.99 | -1.33 | -1.32 | -2.12 | -2.26 | -0.79 | -1.83 | -1 |
| **TRI(N)-Ph** | ***J*** | **-5.61** | -1.07 | -17.73 | -3.7 | -2.66 | -3.89 | -2.14 | -3.26 | -3.88 | -3.09 | -3.91 | -2.63 | -1.46 |

| | | | | | | | | | | | | | |
|---|---|---|---|---|---|---|---|---|---|---|---|---|---|
| | $\Delta E_{spin}$ | **-0.83** | -0.27 | -0.84 | -0.52 | -0.76 | -0.96 | -1.29 | -1.22 | -2.04 | -2.18 | -0.8 | -1.76 | -0.94 |
| **TRI(B) dimer** | ***J*** | **-0.57** | 11.96 | -1.03 | -0.04 | -0.21 | -0.15 | -0.1 | -0.15 | -0.19 | -0.23 | -0.2 | -0.17 | -0.34 |
| | $\Delta E_{spin}$ | **-0.34** | -0.3 | -1 | -0.6 | -0.79 | -1.02 | -1.24 | -1.18 | -1.89 | -1.99 | -0.85 | -1.55 | -0.45 |
| **TRI(B)-CC** | ***J*** | **-3.54** | 5.52 | -0.46 | 0.16 | -0.11 | -0.06 | -0.03 | -0.07 | -0.06 | -0.06 | -0.09 | -0.06 | -0.28 |
| | $\Delta E_{spin}$ | **-0.53** | -0.29 | -0.99 | -0.6 | -0.83 | -1.08 | -1.41 | -1.31 | -2.19 | -2.32 | -0.86 | -1.84 | -0.5 |
| **TRI(B)-CCCC** | ***J*** | **-3.46** | 0.14 | 0.19 | 0.43 | -0.07 | -0.03 | -0.01 | -0.04 | -0.01 | -0.03 | -0.06 | -0.02 | -0.22 |
| | $\Delta E_{spin}$ | **-0.52** | -0.29 | -1 | -0.6 | -0.85 | -1.11 | -1.48 | -1.37 | -2.35 | -2.48 | -0.86 | -2.01 | -0.55 |
| **TRI(B)-Ph** | ***J*** | **-5.12** | 0.39 | -15.88 | -3.74 | -2.64 | -3.67 | -1.96 | -3.17 | -3.48 | -2.77 | -3.74 | -2.4 | -1.26 |
| | $\Delta E_{spin}$ | **-0.67** | -0.29 | -0.98 | -0.59 | -0.81 | -1.06 | -1.4 | -1.3 | -2.22 | -2.35 | -0.93 | -1.88 | -0.49 |
| **TAM-dimer** | ***J*** | **-203** | -267.48 | -170.1 | -181.77 | -152.66 | -144.15 | -126.4 | -136.42 | -110.98 | -107.67 | -157.8 | -100.36 | -106.22 |
| | $\Delta E_{spin}$ | **-0.43** | 0.27 | -0.02 | 0.14 | 0.01 | -0.09 | -0.24 | -0.21 | -0.62 | -0.66 | 0.01 | -0.51 | -0.32 |
| **TAM-CC** | ***J*** | **-127** | -246.6 | -161.33 | -170.19 | -132.47 | -126 | -99.35 | -113.84 | -93.46 | -85.98 | -140 | -85.04 | -90.13 |
| | $\Delta E_{spin}$ | **-0.56** | 0.25 | -0.04 | 0.13 | -0.04 | -0.14 | -0.34 | -0.3 | -0.75 | -0.82 | -0.02 | -0.62 | -0.41 |
| **TAM-CCCC** | ***J*** | **-81** | -191.09 | -133 | -134.34 | -95.41 | -91.97 | -63.44 | -78.78 | -65.42 | -55.99 | -103.69 | -59.45 | -63.07 |
| | $\Delta E_{spin}$ | **-0.79** | 0.19 | -0.1 | 0.07 | -0.13 | -0.24 | -0.52 | -0.45 | -0.97 | -1.07 | -0.1 | -0.81 | -0.57 |
| **TAM-Ph** | ***J*** | **-19** | -49.37 | -53.35 | -34 | -22.07 | -21.35 | -13.83 | -17.92 | -13.39 | -11.7 | -25.04 | -11.43 | -12.34 |
| | $\Delta E_{spin}$ | **-1.16** | 0 | -0.35 | -0.17 | -0.42 | -0.56 | -0.93 | -0.82 | -1.52 | -1.66 | -0.37 | -1.32 | -1.02 |
| **TOT-dimer** | ***J*** | **-74** | -105.9 | -91.64 | -73.91 | -61.45 | -59.69 | -51.99 | -58.46 | -51.84 | -50.82 | -64.96 | -44.96 | -43.52 |
| | $\Delta E_{spin}$ | **-0.53** | 0.09 | -0.33 | -0.05 | -0.22 | -0.34 | -0.57 | -0.5 | -0.98 | -1.06 | -0.22 | -0.82 | -0.6 |

| | | | | | | | | | | | | | | |
|---|---|---|---|---|---|---|---|---|---|---|---|---|---|---|
| **TOT-CC** | ***J*** | **-40** | -104.61 | -92.55 | -73.88 | -55.28 | -53.71 | -40.62 | -49.61 | -43.59 | -40.03 | -59.48 | -38.81 | -38.36 |
| | **$\Delta E_{spin}$** | **-0.68** | 0.09 | -0.33 | -0.05 | -0.24 | -0.37 | -0.65 | -0.56 | -1.1 | -1.2 | -0.22 | -0.92 | -0.68 |
| **TOT-CCCC** | ***J*** | **-17** | -76.23 | -76.58 | -55.32 | -37.24 | -36.86 | -23.78 | -32.33 | -28.46 | -24.13 | -41.41 | -25.27 | -24.97 |
| | **$\Delta E_{spin}$** | **-0.9** | 0.05 | -0.37 | -0.09 | -0.32 | -0.46 | -0.81 | -0.69 | -1.33 | -1.46 | -0.28 | -1.11 | -0.84 |
| **TOT-Ph** | ***J*** | **-11** | -27.09 | -42.88 | -19.16 | -12.87 | -12.53 | -8.29 | -10.94 | -8.9 | -8 | -14.6 | -7.29 | -7.24 |
| | **$\Delta E_{spin}$** | **-1.03** | -0.05 | -0.49 | -0.2 | -0.45 | -0.6 | -0.99 | -0.86 | -1.57 | -1.71 | -0.41 | -1.36 | -1.07 |
| **PLY-dimer** | ***J*** | **-23** | -6.08 | -42.41 | -18.93 | -13.88 | -20.23 | -11.89 | -18.35 | -24.21 | -21.09 | -19.9 | -16.08 | -10.89 |
| | **$\Delta E_{spin}$** | **-1.03** | -0.27 | -0.94 | -0.54 | -0.68 | -0.85 | -1.04 | -1.01 | -1.53 | -1.62 | -0.73 | -1.31 | -1.02 |
| **PLY-CC** | ***J*** | **-8.82** | -4.59 | -42.38 | -17.55 | -11.82 | -17.93 | -9.74 | -15.24 | -21.25 | -17.68 | -17.56 | -14.17 | -9.53 |
| | **$\Delta E_{spin}$** | **-1.15** | -0.31 | -0.99 | -0.58 | -0.78 | -0.97 | -1.26 | -1.2 | -1.89 | -2.02 | -0.8 | -1.65 | -1.32 |
| **PLY-CCCC** | ***J*** | **-6.04** | -2.84 | -32.38 | -11.76 | -7.36 | -11.63 | -5.45 | -9.49 | -13.41 | -10.29 | -11.4 | -8.85 | -5.87 |
| | **$\Delta E_{spin}$** | **-1.21** | -0.31 | -1 | -0.59 | -0.82 | -1.02 | -1.37 | -1.29 | -2.09 | -2.21 | -0.81 | -1.85 | -1.51 |
| **PLY -Ph** | ***J*** | **-4.11** | -0.74 | -17.07 | -2.76 | -1.93 | -3.03 | -1.47 | -2.56 | -3.37 | -2.7 | -3.02 | -2.09 | -1.39 |
| | **$\Delta E_{spin}$** | **-1.0** | -0.31 | -0.99 | -0.59 | -0.81 | -1 | -1.33 | -1.26 | -2.02 | -2.15 | -0.81 | -1.79 | -1.45 |
| **MAE** | ***J*** | | 36.34 | 21.41 | 18.5 | 13.38 | 11.74 | 12.66 | 10.64 | 10.44 | 10.23 | 13.18 | 17.95 | 13.13 |
| | **$\Delta E_{spin}$** | | 0.81 | 0.36 | 0.63 | 0.46 | 0.34 | 0.32 | 0.31 | 0.8 | 0.79 | 0.41 | 0.73 | 0.13 |
| **MRE** | ***J*** | | -1.44 | 1.78 | 0.52 | -0.08 | 0.15 | -0.3 | 0 | 0.16 | -0.03 | 0.2 | 0.36 | -0.25 |
| | **$\Delta E_{spin}$** | | -0.78 | -0.11 | -0.52 | -0.26 | -0.04 | 0.29 | 0.21 | 1.04 | 1.13 | -0.23 | 0.82 | -0.0002 |
| **MARE** | ***J*** | | 2.33 | 2.03 | 0.96 | 0.48 | 0.61 | 0.43 | 0.51 | 0.67 | 0.56 | 0.63 | 1.03 | 0.48 |

| | | | | | | | | | | | | | |
|---|---|---|---|---|---|---|---|---|---|---|---|---|---|
| | $\Delta E_{spin}$ | 0.78 | 0.45 | 0.61 | 0.48 | 0.44 | 0.46 | 0.45 | 1.04 | 1.13 | 0.48 | 0.83 | 0.14 |
| **RMSE** | ***J*** | 72.58 | 26.95 | 37.75 | 36.44 | 26.81 | 29.32 | 24.26 | 21.03 | 22.16 | 29.26 | 38.62 | 27.54 |
| **RMSE** | $\Delta E_{spin}$ | 0.91 | 0.43 | 0.74 | 0.52 | 0.4 | 0.42 | 0.38 | 0.96 | 0.97 | 0.47 | 0.95 | 0.19 |

*In LC-ωPBE, ω=0.4 is default. Here, we tuned the ω for each monomer according to its electron correlations, namely ω=0.20 for TRI, ω=0.15 for TAM, TOT and PLY, ω=0.10 for TRI(N) and ω=0.05 for TRI(B).

## ASSOCIATED CONTENT

**Supporting Information**. This material is available free of charge via the Internet at http://pubs.acs.org. natural orbitals in active space of all the molecules in the dataset as well as the comparison of the DFT results for ORCA and Gaussian16 programs.

## AUTHOR INFORMATION


### Corresponding Author

**Thomas Heine**: Faculty of Chemistry and Food Chemistry, TU Dresden, 01069 Dresden, Germany; Institute of Resource Ecology, Helmholtz-Zentrum Dresden-Rossendorf, 04316 Leipzig, Germany; Department of Chemistry, Yonsei University, Seoul 120-749, Korea;

ORCID: 0000-0003-2379-6251;

Email: thomas.heine@tu-dresden.de

### Authors

**Hongde Yu**: Faculty of Chemistry and Food Chemistry, TU Dresden, 01069 Dresden, Germany;

ORCID: 0000-0002-2576-271X;

Email: hongde.yu@mailbox.tu-dresden.de

**Jianwei Sun**: Department of Physics and Engineering Physics, Tulane University, New Orleans, Louisiana 70118, United States;

ORCID: 0000-0002-2361-6823;

Email: jsun@tulane.edu


### Notes

The authors declare no competing financial interest.

## ACKNOWLEDGMENTS


We thank the Center for Information Services and High-Performance Computing (ZIH) at TU Dresden for computational resources. Financial support by the Alexander von Humboldt Foundation is acknowledged. We thank Deutsche Forschungsgemeinschaft, CRC 1415, for continuing support.

**References:**


(1) Miller, J. S., Magnetically ordered molecule-based materials. *Chem. Soc. Rev.* **2011,** *40*, 3266-3296.

(2) Mahmood, J.; Baek, J.-B., Room-Temperature Organic Ferromagnetism. *Chem* **2019,** *5*, 1012-1014.

(3) Jin, E.; Asada, M.; Xu, Q.; Dalapati, S.; Addicoat, M. A.; Brady, M. A.; Xu, H.; Nakamura, T.; Heine, T.; Chen, Q.; Jiang, D., Two-dimensional $sp^2$ carbon-conjugated covalent organic frameworks. *Science* **2017,** *357*, 673-676.

(4) Wu, S.; Li, M.; Phan, H.; Wang, D.; Herng, T. S.; Ding, J.; Lu, Z.; Wu, J., Toward Two-Dimensional π-Conjugated Covalent Organic Radical Frameworks. *Angew. Chem. Int. Ed.* **2018,** *57*, 8007-8011.

(5) Abe, M., Diradicals. *Chem. Rev.* **2013,** *113*, 7011-7088.

(6) Malrieu, J. P.; Caballol, R.; Calzado, C. J.; De Graaf, C.; Guihery, N., Magnetic interactions in molecules and highly correlated materials: physical content, analytical derivation, and rigorous extraction of magnetic Hamiltonians. *Chem. Rev.* **2014,** *114*, 429-492.

(7) Angeli, C.; Cimiraglia, R.; Evangelisti, S.; Leininger, T.; Malrieu, J.-P., Introduction of n-electron valence states for multireference perturbation theory. *J. Chem. Phys.* **2001,** *114*, 10252-10264.

(8) Zhou, C.; Hermes, M.; Wu, D.; Bao, J. J.; Pandharkar, R.; King, D. R.; Zhang, D.; Scott, T.; Lykhin, A.; Gagliardi, L., Electronic structure of strongly correlated systems: recent developments in multiconfiguration pair-density functional theory and multiconfiguration nonclassical-energy functional theory. *Chem. Sci.* **2022**.

(9) Sharma, P.; Truhlar, D. G.; Gagliardi, L., Magnetic coupling in a tris-hydroxo-bridged chromium dimer occurs through ligand mediated superexchange in conjunction with through-space coupling. *J. Am. Chem. Soc.* **2020,** *142*, 16644-16650.

(10) White, S. R., Density matrix formulation for quantum renormalization groups. *Phys. Rev. Lett.* **1992,** *69*, 2863.

(11) Kurashige, Y.; Yanai, T., Second-order perturbation theory with a density matrix renormalization group self-consistent field reference function: Theory and application to the study of chromium dimer. *J. Chem. Phys.* **2011,** *135*, 094104.

(12) Olivares-Amaya, R.; Hu, W.; Nakatani, N.; Sharma, S.; Yang, J.; Chan, G. K.-L., The ab-initio density matrix renormalization group in practice. *J. Chem. Phys.* **2015,** *142*, 034102.

(13) Li, J.; Jin, Y.; Rinke, P.; Yang, W.; Golze, D., Benchmark of GW methods for core-level binding energies. *J. Chem. Theory Comput.* **2022,** *18*, 7570-7585.

(14) Reining, L., The GW approximation: content, successes and limitations. *Wiley Interdiscip. Rev. Comput. Mol. Sci.* **2018,** *8*, e1344.

(15) Ren, X.; Rinke, P.; Blum, V.; Wieferink, J.; Tkatchenko, A.; Sanfilippo, A.; Reuter, K.; Scheffler, M., Resolution-of-identity approach to Hartree–Fock, hybrid density functionals, RPA, MP2 and GW with numeric atom-centered orbital basis functions. *New J. Phys.* **2012,** *14*, 053020.

(16) Eshuis, H.; Bates, J. E.; Furche, F., Electron correlation methods based on the random phase approximation. *Theor. Chem. Acc.* **2012,** *131*, 1-18.

(17) Anisimov, V. I.; Aryasetiawan, F.; Lichtenstein, A., First-principles calculations of the electronic structure and spectra of strongly correlated systems: the LDA+ U method. *J. Condens. Matter Phys.* **1997,** *9*, 767.
(18) Pavliček, N.; Mistry, A.; Majzik, Z.; Moll, N.; Meyer, G.; Fox, D. J.; Gross, L., Synthesis and characterization of triangulene. *Nat. Nanotechnol.* **2017,** *12*, 308-311.
(19) Mishra, S.; Beyer, D.; Eimre, K.; Ortiz, R.; Fernández-Rossier, J.; Berger, R.; Gröning, O.; Pignedoli, C. A.; Fasel, R.; Feng, X., Collective all-carbon magnetism in triangulene dimers. *Angew. Chem. Int. Ed.* **2020,** *132*, 12139-12145.
(20) Hieulle, J.; Castro, S.; Friedrich, N.; Vegliante, A.; Lara, F. R.; Sanz, S.; Rey, D.; Corso, M.; Frederiksen, T.; Pascual, J. I., On-Surface Synthesis and Collective Spin Excitations of a Triangulene-Based Nanostar. *Angew. Chem. Int. Ed.* **2021,** *60*, 25224-25229.
(21) Wang, T.; Berdonces-Layunta, A.; Friedrich, N.; Vilas-Varela, M.; Calupitan, J. P.; Pascual, J. I.; Peña, D.; Casanova, D.; Corso, M.; de Oteyza, D. G., Aza-Triangulene: On-Surface Synthesis and Electronic and Magnetic Properties. *J. Am. Chem. Soc.* **2022,** *144*, 4522-4529.
(22) Jing, Y.; Heine, T., Two-dimensional kagome lattices made of hetero triangulenes are Dirac semimetals or single-band semiconductors. *J. Am. Chem. Soc.* **2018,** *141*, 743-747.
(23) Galeotti, G.; De Marchi, F.; Hamzehpoor, E.; MacLean, O.; Rajeswara Rao, M.; Chen, Y.; Besteiro, L.; Dettmann, D.; Ferrari, L.; Frezza, F., Synthesis of mesoscale ordered two-dimensional π-conjugated polymers with semiconducting properties. *Nat. Mater.* **2020,** *19*, 874-880.
(24) Mishra, S.; Catarina, G.; Wu, F.; Ortiz, R.; Jacob, D.; Eimre, K.; Ma, J.; Pignedoli, C. A.; Feng, X.; Ruffieux, P., Observation of fractional edge excitations in nanographene spin chains. *Nature* **2021,** *598*, 287-292.
(25) Ortiz, R.; Boto, R. A.; García-Martínez, N.; Sancho-García, J. C.; Melle-Franco, M.; Fernández-Rossier, J. n., Exchange rules for diradical π-conjugated hydrocarbons. *Nano Lett.* **2019,** *19*, 5991-5997.
(26) Savarese, M.; Brémond, E.; Ciofini, I.; Adamo, C., Electron Spin Densities and Density Functional Approximations: Open-Shell Polycyclic Aromatic Hydrocarbons as Case Study. *J. Chem. Theory Comput.* **2020,** *16*, 3567-3577.
(27) de PR Moreira, I.; Illas, F., A unified view of the theoretical description of magnetic coupling in molecular chemistry and solid state physics. *Phys. Chem. Chem. Phys.* **2006,** *8*, 1645-1659.
(28) Mori, T., *Electronic properties of organic conductors*. Springer: 2016.
(29) Guo, Y.; Riplinger, C.; Becker, U.; Liakos, D. G.; Minenkov, Y.; Cavallo, L.; Neese, F., Communication: An improved linear scaling perturbative triples correction for the domain based local pair-natural orbital based singles and doubles coupled cluster method [DLPNO-CCSD (T)]. *J. Chem. Phys.* **2018,** *148*, 011101.
(30) Neese, F., The ORCA program system. *Wiley Interdiscip. Rev. Comput. Mol. Sci.* **2012,** *2*, 73-78.
(31) Mishra, S.; Beyer, D.; Eimre, K.; Kezilebieke, S.; Berger, R.; Gröning, O.; Pignedoli, C. A.; Müllen, K.; Liljeroth, P.; Ruffieux, P., Topological frustration induces

unconventional magnetism in a nanographene. *Nat. Nanotechnol.* **2020,** *15*, 22-28.
(32) Hieulle, J.; Castro, S.; Friedrich, N.; Vegliante, A.; Lara, F. R.; Sanz, S.; Rey, D.; Corso, M.; Frederiksen, T.; Pascual, J. I.; Peña, D., On-surface synthesis and collective spin excitations of a triangulene-based nanostar. *Angew. Chem. Int. Ed.* **2021,** *60*, 25224-25229.
(33) Noodleman, L.; Davidson, E. R., Ligand spin polarization and antiferromagnetic coupling in transition metal dimers. *Chem. Phys.* **1986,** *109*, 131-143.
(34) Noodleman, L., Valence bond description of antiferromagnetic coupling in transition metal dimers. *J. Chem. Phys.* **1981,** *74*, 5737-5743.
(35) Nagao, H.; Nishino, M.; Shigeta, Y.; Soda, T.; Kitagawa, Y.; Onishi, T.; Yoshioka, Y.; Yamaguchi, K., Theoretical studies on effective spin interactions, spin alignments and macroscopic spin tunneling in polynuclear manganese and related complexes and their mesoscopic clusters. *Coord. Chem. Rev.* **2000,** *198*, 265-295.
(36) Ruiz, E.; Alvarez, S.; Cano, J.; Polo, V., About the calculation of exchange coupling constants using density-functional theory: The role of the self-interaction error. *J. Chem. Phys.* **2005,** *123*, 164110.
(37) Singh, G.; Gamboa, S.; Orio, M.; Pantazis, D. A.; Roemelt, M., Magnetic exchange coupling in Cu dimers studied with modern multireference methods and broken-symmetry coupled cluster theory. *Theor. Chem. Acc.* **2021,** *140*, 1-15.
(38) Cramer, C. J.; Truhlar, D. G., Density functional theory for transition metals and transition metal chemistry. *Phys. Chem. Chem. Phys.* **2009,** *11*, 10757-10816.
(39) Phillips, J. J.; Peralta, J. E., Towards the blackbox computation of magnetic exchange coupling parameters in polynuclear transition-metal complexes: Theory, implementation, and application. *J. Chem. Phys.* **2013,** *138*, 174115.
(40) Shoji, M.; Koizumi, K.; Kitagawa, Y.; Kawakami, T.; Yamanaka, S.; Okumura, M.; Yamaguchi, K., A general algorithm for calculation of Heisenberg exchange integrals J in multispin systems. *Chem. Phys. Lett.* **2006,** *432*, 343-347.
(41) Yamanaka, S.; Okumura, M.; Nakano, M.; Yamaguchi, K., EHF theory of chemical reactions part 4. UNO CASSCF, UNO CASPT2 and R (U) HF coupled-cluster (CC) wavefunctions. *J. Mol. Struct.* **1994,** *310*, 205-218.
(42) Adamo, C.; Barone, V.; Bencini, A.; Broer, R.; Filatov, M.; Harrison, N.; Illas, F.; Malrieu, J.; de PR Moreira, I., Comment on "About the calculation of exchange coupling constants using density-functional theory: The role of the self-interaction error"[J. Chem. Phys. 123, 164110 (2005)]. *J. Chem. Phys.* **2006,** *124*, 107101.
(43) Bencini, A.; Totti, F., A few comments on the application of density functional theory to the calculation of the magnetic structure of oligo-nuclear transition metal clusters. *J. Chem. Theory Comput.* **2009,** *5*, 144-154.
(44) Perdew, J. P.; Burke, K.; Ernzerhof, M., Generalized gradient approximation made simple. *Phys. Rev. Lett.* **1996,** *77*, 3865.
(45) Becke, A. D., Density-functional exchange-energy approximation with correct asymptotic behavior. *Phys. Rev. A* **1988,** *38*, 3098.
(46) Lee, C.; Yang, W.; Parr, R. G., Development of the Colle-Salvetti correlation-energy formula into a functional of the electron density. *Phys. Rev. B* **1988,** *37*, 785.
(47) Perdew, J. P., Density-functional approximation for the correlation energy of the

inhomogeneous electron gas. *Phys. Rev. B* **1986,** *33*, 8822.
(48) Tao, J.; Perdew, J. P.; Staroverov, V. N.; Scuseria, G. E., Climbing the density functional ladder: Nonempirical meta–generalized gradient approximation designed for molecules and solids. *Phys. Rev. Lett.* **2003,** *91*, 146401.
(49) Zhao, Y.; Truhlar, D. G., A new local density functional for main-group thermochemistry, transition metal bonding, thermochemical kinetics, and noncovalent interactions. *J. Chem. Phys.* **2006,** *125*, 194101.
(50) Sun, J.; Ruzsinszky, A.; Perdew, J. P., Strongly constrained and appropriately normed semilocal density functional. *Phys. Rev. Lett.* **2015,** *115*, 036402.
(51) Grimme, S.; Hansen, A.; Ehlert, S.; Mewes, J.-M., $r^2$SCAN-3c: A "Swiss army knife" composite electronic-structure method. *J. Chem. Phys.* **2021,** *154*, 064103.
(52) Zhao, Y.; Truhlar, D. G., The M06 suite of density functionals for main group thermochemistry, thermochemical kinetics, noncovalent interactions, excited states, and transition elements: two new functionals and systematic testing of four M06-class functionals and 12 other functionals. *Theor. Chem. Acc.* **2008,** *120*, 215-241.
(53) Becke, A., Density-functional thermochemistry. III The role of exact exchange *J. Chem. Phys.* **1993,** *98*, 5648.
(54) Adamo, C.; Barone, V., Toward reliable density functional methods without adjustable parameters: The PBE0 model. *J. Chem. Phys.* **1999,** *110*, 6158-6170.
(55) Haoyu, S. Y.; He, X.; Li, S. L.; Truhlar, D. G., MN15: A Kohn–Sham global-hybrid exchange–correlation density functional with broad accuracy for multi-reference and single-reference systems and noncovalent interactions. *Chem. Sci.* **2016,** *7*, 5032-5051.
(56) Zhao, Y.; Truhlar, D. G., Design of density functionals that are broadly accurate for thermochemistry, thermochemical kinetics, and nonbonded interactions. *J. Phys. Chem. A* **2005,** *109*, 5656-5667.
(57) Chai, J.-D.; Head-Gordon, M., Long-range corrected hybrid density functionals with damped atom–atom dispersion corrections. *Phys. Chem. Chem. Phys.* **2008,** *10*, 6615-6620.
(58) Mardirossian, N.; Head-Gordon, M., ωB97M-V: A combinatorially optimized, range-separated hybrid, meta-GGA density functional with VV10 nonlocal correlation. *J. Chem. Phys.* **2016,** *144*, 214110.
(59) Heyd, J.; Scuseria, G. E.; Ernzerhof, M., Hybrid functionals based on a screened Coulomb potential. *J. Chem. Phys.* **2003,** *118*, 8207-8215.
(60) Karton, A.; Tarnopolsky, A.; Lamére, J.-F.; Schatz, G. C.; Martin, J. M., Highly accurate first-principles benchmark data sets for the parametrization and validation of density functional and other approximate methods. Derivation of a robust, generally applicable, double-hybrid functional for thermochemistry and thermochemical kinetics. *J. Phys. Chem. A* **2008,** *112*, 12868-12886.
(61) Goerigk, L.; Grimme, S., Efficient and Accurate Double-Hybrid-Meta-GGA Density Functionals-Evaluation with the Extended GMTKN30 Database for General Main Group Thermochemistry, Kinetics, and Noncovalent Interactions. *J. Chem. Theory Comput.* **2011,** *7*, 291-309.
(62) Grimme, S., Semiempirical hybrid density functional with perturbative second-order correlation. *J. Chem. Phys.* **2006,** *124*, 034108.

(63) Chai, J.-D.; Head-Gordon, M., Systematic optimization of long-range corrected hybrid density functionals. *J. Chem. Phys.* **2008,** *128*, 084106.
(64) Pantazis, D. A., Assessment of double-hybrid density functional theory for magnetic exchange coupling in manganese complexes. *Inorganics* **2019,** *7*, 57.
(65) Kaur, P.; Ali, M. E., First principle investigations of long-range magnetic exchange interactions via polyacene couplers. *Int. J. Quantum Chem.* **2021,** *121*, e26756.
(66) Khurana, R.; Bajaj, A.; Ali, M. E., Tuning the magnetic properties of a diamagnetic di-Blatter's zwitterion to antiferro-and ferromagnetically coupled diradicals. *Phys. Chem. Chem. Phys.* **2022,** *24*, 2543-2553.
(67) Bajaj, A.; Khurana, R.; Ali, M. E., Auxiliary atomic relay center facilitates enhanced magnetic couplings in Blatter's radical. *J. Phys. Chem. A* **2021,** *125*, 4133-4142.
(68) Ko, K. C.; Cho, D.; Lee, J. Y., Scaling approach for intramolecular magnetic coupling constants of organic diradicals. *J. Phys. Chem. A* **2013,** *117*, 3561-3568.
(69) Cho, D.; Ko, K. C.; Ikabata, Y.; Wakayama, K.; Yoshikawa, T.; Nakai, H.; Lee, J. Y., Effect of Hartree-Fock exact exchange on intramolecular magnetic coupling constants of organic diradicals. *J. Chem. Phys.* **2015,** *142*, 024318.
(70) Moreira, I. d. P.; Costa, R.; Filatov, M.; Illas, F., Restricted ensemble-referenced Kohn− Sham versus broken symmetry approaches in density functional theory: magnetic coupling in cu binuclear complexes. *J. Chem. Theory Comput.* **2007,** *3*, 764-774.
(71) Gusev, A.; Nemec, I.; Herchel, R.; Riush, I.; Titiš, J.; Boča, R.; Lyssenko, K.; Kiskin, M.; Eremenko, I.; Linert, W., Structural and magnetic characterization of Ni (II), Co (II), and Fe (II) binuclear complexes on a bis (pyridyl-triazolyl) alkane basis. *Dalton Trans.* **2019,** *48*, 10526-10536.
(72) Massoud, S. S.; Junk, T.; Louka, F. R.; Herchel, R.; Trávníček, Z.; Fischer, R. C.; Mautner, F. A., Synthesis, structure and magnetic characterization of dinuclear copper (II) complexes bridged by bicompartmental phenolate. *RSC Adv.* **2015,** *5*, 87139-87150.
(73) Pandey, L.; Doiron, C.; Sears, J. S.; Brédas, J.-L., Lowest excited states and optical absorption spectra of donor–acceptor copolymers for organic photovoltaics: a new picture emerging from tuned long-range corrected density functionals. *Phys. Chem. Chem. Phys.* **2012,** *14*, 14243-14248.
(74) Rivero, P.; de PR Moreira, I.; Scuseria, G. E.; Illas, F., Description of magnetic interactions in strongly correlated solids via range-separated hybrid functionals. *Phys. Rev. B* **2009,** *79*, 245129.
(75) Vydrov, O. A.; Heyd, J.; Krukau, A. V.; Scuseria, G. E., Importance of short-range versus long-range Hartree-Fock exchange for the performance of hybrid density functionals. *J. Chem. Phys.* **2006,** *125*, 074106.
(76) Vydrov, O. A.; Scuseria, G. E., Assessment of a long-range corrected hybrid functional. *J. Chem. Phys.* **2006,** *125*, 234109.
(77) Peralta, J. E.; Melo, J. I., Magnetic exchange couplings with range-separated hybrid density functionals. *J. Chem. Theory Comput.* **2010,** *6*, 1894-1899.
(78) Stein, T.; Kronik, L.; Baer, R., Reliable prediction of charge transfer excitations in molecular complexes using time-dependent density functional theory. *J. Am. Chem. Soc.*

**2009,** *131*, 2818-2820.
(79) Li, J.; Chen, Z.; Yang, W., Multireference Density Functional Theory for Describing Ground and Excited States with Renormalized Singles. *J. Phys. Chem. Lett.* **2022,** *13*, 894-903.
(80) Fromager, E.; Gidopoulos, N.; Gori-Giorgi, P.; Helgaker, T.; Loos, P.-F.; Malcomson, T.; Pernal, K.; Savin, A.; Truhlar, D. G.; Wibowo, M., Strong correlation in density functional theory: general discussion. *Faraday Discuss.* **2020,** *224*, 373-381.
(81) Li Manni, G.; Carlson, R. K.; Luo, S.; Ma, D.; Olsen, J.; Truhlar, D. G.; Gagliardi, L., Multiconfiguration pair-density functional theory. *J. Chem. Theory Comput.* **2014,** *10*, 3669-3680.
(82) Frisch, M. J.; Trucks, G. W.; Schlegel, H. B.; Scuseria, G. E.; Robb, M. A.; Cheeseman, J. R.; Scalmani, G.; Barone, V.; Petersson, G. A.; Nakatsuji, H.; Li, X.; Caricato, M.; Marenich, A. V.; Bloino, J.; Janesko, B. G.; Gomperts, R.; Mennucci, B.; Hratchian, H. P.; Ortiz, J. V.; Izmaylov, A. F.; Sonnenberg, J. L.; Williams; Ding, F.; Lipparini, F.; Egidi, F.; Goings, J.; Peng, B.; Petrone, A.; Henderson, T.; Ranasinghe, D.; Zakrzewski, V. G.; Gao, J.; Rega, N.; Zheng, G.; Liang, W.; Hada, M.; Ehara, M.; Toyota, K.; Fukuda, R.; Hasegawa, J.; Ishida, M.; Nakajima, T.; Honda, Y.; Kitao, O.; Nakai, H.; Vreven, T.; Throssell, K.; Montgomery Jr., J. A.; Peralta, J. E.; Ogliaro, F.; Bearpark, M. J.; Heyd, J. J.; Brothers, E. N.; Kudin, K. N.; Staroverov, V. N.; Keith, T. A.; Kobayashi, R.; Normand, J.; Raghavachari, K.; Rendell, A. P.; Burant, J. C.; Iyengar, S. S.; Tomasi, J.; Cossi, M.; Millam, J. M.; Klene, M.; Adamo, C.; Cammi, R.; Ochterski, J. W.; Martin, R. L.; Morokuma, K.; Farkas, O.; Foresman, J. B.; Fox, D. J. *Gaussian 16 Rev. C.01*, Wallingford, CT, 2016.
(83) Weigend, F., Accurate Coulomb-fitting basis sets for H to Rn. *Phys. Chem. Chem. Phys.* **2006,** *8*, 1057-1065.
(84) Helmich-Paris, B., Benchmarks for electronically excited states with CASSCF methods. *J. Chem. Theory Comput.* **2019,** *15*, 4170-4179.
(85) Neese, F.; Wennmohs, F.; Hansen, A.; Becker, U., Efficient, approximate and parallel Hartree–Fock and hybrid DFT calculations. A 'chain-of-spheres' algorithm for the Hartree–Fock exchange. *Chem. Phys.* **2009,** *356*, 98-109.
(86) Aravena, D.; Atanasov, M.; Chilkuri, V.; Guo, Y.; Jung, J.; Maganas, D.; Mondal, B.; Schapiro, I.; Sivalingam, K.; Ye, S., CASSCF Calculations in ORCA (4.2): A tutorial Introduction. *https://orcaforum.kofo.mpg.de/app.php/dlext/?cat=4*.
(87) Weigend, F.; Ahlrichs, R., Balanced basis sets of split valence, triple zeta valence and quadruple zeta valence quality for H to Rn: Design and assessment of accuracy. *Phys. Chem. Chem. Phys.* **2005,** *7*, 3297-3305.

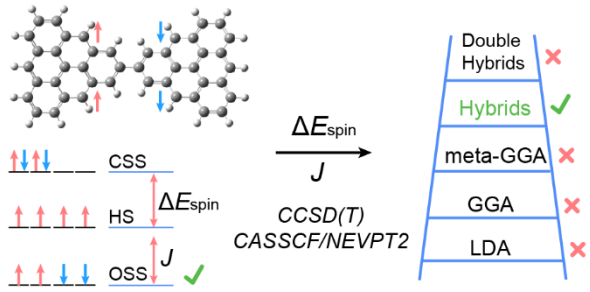
CSS
HS
OSS
ΔEspin
J
ΔEspin
J
CCSD(T)
CASSCF/NEVPT2
Double Hybrids
Hybrids
meta-GGA
GGA
LDA